Evidence for Protracted Intracrustal Reworking of Palaeoarchaean Crust in the Pilbara Craton (Mount Edgar Dome, Western Australia)

Anda Buzenchi, Hugo Moreira, Olivier Bruguier, Bruno Dhuime

GeoScienceWorld
Lithosphere
Volume 2022, Article ID 3808313, 19 pages
https://doi.org/10.2113/2022/3808313

Lithosphere

Research Article

Evidence for Protracted Intracrustal Reworking of Palaeoarchaean Crust in the Pilbara Craton (Mount Edgar Dome, Western Australia)

Anda Buzenchi, Hugo Moreira, Olivier Bruguier, and Bruno Dhuime

CNRS & Université de Montpellier, Géosciences Montpellier, France

Correspondence should be addressed to Anda Buzenchi; anda-ioana.buzenchi@umontpellier.fr

Received 21 February 2022; Accepted 30 June 2022; Published 12 August 2022

Academic Editor: Nasipuri Pritam

~3.5-2.8 Ga granitoids from the Pilbara Craton in Western Australia are one of the most ancient and best-preserved records of early processes of continental crust generation. A number of recent studies have focused on the nature of the mantle source from which Pilbara granitoids derived, yet no consensus has been reached on whether the mantle was chondritic or depleted in the Eo/Palaeoarchaean. Here we present integrated whole-rock (major and trace elements) and zircon (U-Pb and Lu-Hf isotopes) data for 10 granitoids sampled across the Mount Edgar Dome, which recorded four main magmatic events between 3.47 and 3.23 Ga. Whole-rock major and trace element analyses suggest that the samples belong to two distinct petrogenetic groups. The first group is akin to the tonalite-trondhjemite-granodiorite (TTG) suite, representing highly fractionated magmas initially formed by partial melting of a basaltic crust. The second group, here classified as granites, is best interpreted by the remelting of a basaltic crust and the addition of more evolved material, and it is striking that TTG-like and granitic magmas occurred coevally in time and space. Overall, both groups were formed through intense intracrustal differentiation processes that lead to the loss of significant geochemical information about their original sources. High-precision Lu-Hf analyses in zircon allow to obtain such information and to trace back the isotopic composition of the Palaeoarchaean mantle. A clear change from superchondritic to subchondritic Hf isotope compositions is observed between 3.47 and 3.23 Ga. The superchondritic Hf isotope composition of the 3.47 Ga old granitoids substantiates derivation from a depleted mantle source that separated from the chondritic mantle prior to 3.8 Ga. The presence of ca. 3.5 Ga old inherited zircons in younger magmas suggests that crustal remelting processes were involved in their generation. We propose that all granitoids investigated in this study had their crustal sources originated from a single mantle–crust differentiation event that occurred at 3.50 Ga. This event resulted in the differentiation, from the same original mantle, of two distinct crustal reservoirs, i.e., a mafic reservoir with a $^{176}Lu/^{177}Hf$ ratio of 0.023, and a reservoir of intermediate/felsic composition ($^{176}Lu/^{177}Hf = 0.013$). 3.32-3.31 Ga-old granitoids were produced by remelting of the mafic reservoir, whereas 3.43 and 3.23 Ga granitoids derived from the intermediate/felsic reservoir. Overall, our data suggest that protracted intracrustal remelting processes and differentiation have played a key role in the formation, evolution, and maturation of the building blocks of continents during the Palaeoarchaean.

1. Introduction

The earliest magmatic record is scarce, and the hunt for rocks and minerals that preserve primary geochemical signatures after multiple episodes of crust generation and differentiation provides key information on the first stages of Earth's evolution (e.g., [1–5]). Amongst ancient rocks that are still preserved on Earth's surface, Archaean granitoids are of major interest because they record the development of the first continents and were involved in lithosphere cratonisation (e.g., [6, 7]). The early evolved (i.e., SiO_2-rich) crust was essentially made of tonalite-trondhjemite-granodiorite (TTG) rocks, i.e., silica-sodium-rich magmas with high Sr/Y and La/Yb ratios [8, 9]. It is widely assumed that TTGs derived from a mafic precursor and, as such, are the building blocks of the continental crust and a link to the earliest mantle–crust differentiation processes [10–13]. It is however unclear how the remnants of ancient

continents exposed in cratons worldwide were formed, and which tectonic settings were associated with the production of large volumes of new continental crust [14–20].

The existence of an early evolved crust implies the presence of a complementary depleted reservoir within the mantle, and there is an ongoing debate over the size and the rate of depletion of the depleted mantle (DM). Some authors have suggested that the mantle suffered a progressive depletion in incompatible elements due to crustal extraction from the Hadean (i.e., >4 Ga) [20–23], while others have proposed that early continental crust was essentially formed from a mantle with a broadly chondritic composition, and that mantle depletion started to be significant only from the Mesoarchaean [5, 14, 24–27].

The East Pilbara Terrane (EPT) of the Pilbara Craton in Western Australia constitutes an exceptionally well-preserved segment ancient continental crust, which has long remained at the centre of debates on the nature of the early crust and mantle. The EPT contains several plutonic bodies that range in age from 3.59 to 2.8 Ga [28–32] and which have classically been interpreted to derive from an ancient protocrust (>3.8 Ga) that was repeatedly reworked with limited input of juvenile mantle material [31, 33–35]. In contrast, recent lines of evidences have suggested that progressive juvenile additions have played a key role in the formation and evolution of the EPT crust [26, 27, 32].

In order to better constrain the nature of the mantle reservoir from which Archaean granitoids derived, this study focuses on the evolution one dome of the EPT, i.e., the Mount Edgar Granitic Complex (MEGC). The MEGC offers one of the most complete records of Palaeoarchaean magmatic events in the EPT. We present new U-Pb and Lu-Hf isotope analyses in zircon, in combination with whole-rock geochemistry, for 10 samples from four Supersuites sampled across the MEGC (Callina, Tambina, Emu Pool, and Cleland) and with crystallisation ages ranging 3.47-3.23 Ga. We show that TTG-like and granitic melts occurred coevally in time and space, and that the geochemical change towards TTG and more evolved granitic composition was achieved by intracrustal differentiation processes. We propose a simple evolution model in which a major crust generation event from a depleted mantle source occurred at around 3.50 Ga, most likely in a vertical tectonics regime, and which generated two crustal reservoirs that evolved independently from each other from their extraction until at least 3.23 Ga.

2. Geological Setting

The East Pilbara Terrane (EPT) is part of the Pilbara Craton in Western Australia. It is exposed for more than 40,000 km^2, and it represents a classical example of an Archaean granite-greenstone belt [36], with large granitic domes flanked by supracrustal greenstone belts and together forming a dome-and-keel architecture [37] (Figure 1).

The granitic domes of the EPT were formed by magmatic pulses over several hundred million years. Major magmatic events occurred between c. 3.53 Ga and 3.22 Ga [11], with five distinct pulses associated with the following "Supersuites": Mulgundoona (3.53-3.49 Ga) [26, 32, 35], Callina (3.48-3.46 Ga), Tambina (3.45-3.42 Ga), Emu Pool (3.32-3.28 Ga), Cleland (3.27-3.22 Ga) [28, 39], and Split Rock (2.85-2.83 Ga) [31]. The greenstone belts are composed of intercalated ultramafic, mafic, and minor felsic lithologies, which are Palaeoarchaean in age and contemporaneous to granitic intrusions in the EPT [11, 31, 40, 41]. The oldest group of greenstone belts, Warrawoona (3.53-3.42 Ga), is dominated by ultramafic-mafic lithologies. The younger Kelly and Sulphur Springs groups (3.35-3.31 Ga and 3.29-3.23 Ga, respectively) are formed by ultramafic-mafic-felsic lithologies in which the proportion of felsic material increases with time [31, 38].

The Palaeoarchaean to Mesoarchaean tectonic evolution of the EPT is marked by various episodes of major vertical uplift and deformation events, which have been related to diapiric doming and to the subsidence of the greenstone basins [11, 12, 37, 42, 43]. Doming events occurred between 3.49 to 3.29 Ga and coincide with periods of granitic intrusions [11, 40, 43, 44]. The last Archaean tectonic events recorded in the EPT reflect crustal extension, rifting, and break-up at c. 3.22 Ga. These events were subsequently followed by Mesoarchaean crustal evolution processes associated to horizontal tectonics [36, 40, 45].

This study focuses on the Mount Edgar Dome (MED) within the EPT. The MED is located at the core of the EPT and shows a circular exposure of approximatively 50 km in diameter. It comprises granitic rocks belonging to the Callina, Tambina, Emu Pool, Cleland, and Split Rock Supersuites, together forming the Mount Edgar Granitic Complex (MEGC). The 3.48-3.46 Ga Callina Supersuite is composed dominantly of granodiorites, with less abundant biotite-tonalites and trondhjemites. Rocks from the 3.45-3.42 Ga Tambina Supersuite are predominantly sodic, with abundant tonalites and granodiorites. Previous studies interpreted the TTG magmas of these two Supersuites to derive either from intracrustal melting of an enriched basaltic crust [46] or of an older felsic crust [47]. The Emu Pool Supersuite comprises widespread and voluminous intrusions of monzogranite and granodiorite dated between 3.32 and 3.28 Ga. The full compositional range of this Supersuite extends from trondhjemite to syenogranite. Several distinct compositional plutons have been identified in the Corunna Downs, Mount Edgar, Muccan, Warrawagine, and Yilgalong Domes, and the intrusions are only moderately to weakly foliated. The granitic rocks from this Supersuite derived from the partial melting of either a juvenile mafic source [26, 27] or an older granitic crust [46, 48–50]. Granitic rocks from the Cleland Supersuite intruded most domes of the EPT between 3.27 and 3.22 Ga. They are dominantly monzogranitic in composition, with granodiorites and syenogranites locally present, and they are believed to derive from the melting of an older granitic crust [30, 46, 49]. After a 37 million years hiatus in the magmatic record, the Split Rock Supersuite, which contains highly fractionated, post-tectonic monzogranite to syenogranite plutons, was emplaced between 2.85 and 2.83 Ga [30]. The outer margin of the MEGC is surrounded by the 3.53-2.95 Ga Marble Bar greenstone belt. To the East, the contacts with the MED are concealed by the 2.78-2.63 Ga Fortescue Basin.

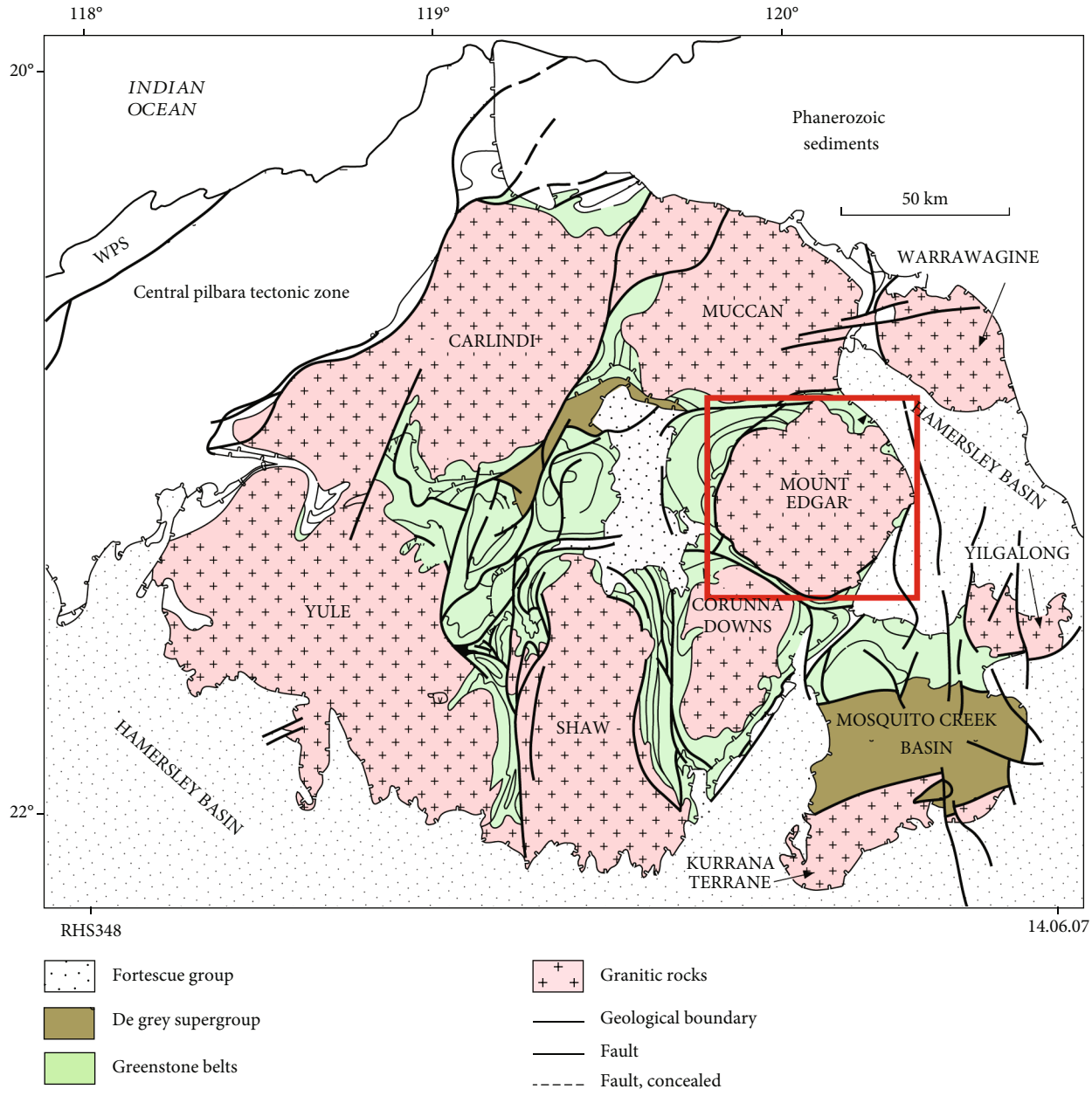

FIGURE 1: Geological map of the East Pilbara Terrane in Western Australia, simplified after [38]. Red rectangle highlights the studied area (see Figure 2).

3. Samples and Analytical Techniques

Nondeformed to weakly foliated granitoids were collected across the MED during a fieldtrip in 2017. Ten samples were selected for this study: two samples from the 3.48-3.46 Ga Callina Supersuite (WA17-35 and WA17-31), one sample from the 3.45-3.42 Ga Tambina Supersuite (WA17-37), 6 samples from the 3.33-3.32 Ga Emu Pool Supersuite (WA17-30, WA17-32, WA17-36, WA17-33, WA17-34, and WA17-27), and one sample from the 3.27-3.22 Ga Cleland Supersuite (WA17-28). The location of the samples is shown in Figure 2, a summary of their petrography is given in Table 1, and detailed petrographic descriptions are available in Supplementary File 4.

Major and trace element analyses of whole-rock powders were performed at the SRAM (Service d'Analyse des Roches et Minéraux, Nancy, France) following the procedure described in Carignan et al. [51]. Rock preparation and mineral separation were done at the Montpellier University. For mineral separation, about 1 kg of each sample was crushed using a jaw crusher and a disc mill and subsequently sieved to keep the 50-300 μm size fraction. Zircons were then concentrated using magnetic separator and heavy liquids. About 20 grains were hand-picked for each sample, set in 1-inch epoxy mounts and polished to expose internal structures. Zircon images were acquired at Montpellier University, using a FEI Quanta 200 FEG Scanning Electron Microscope (SEM) equipped with cathodoluminescence (CL) and back-

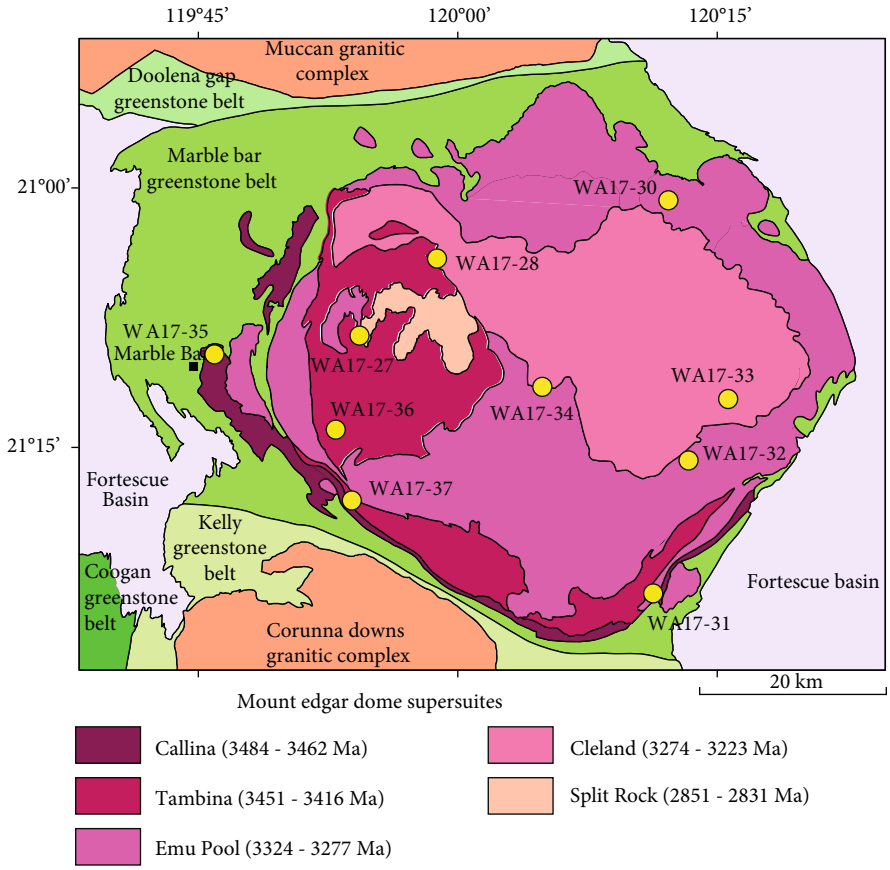

FIGURE 2: Simplified geological map of the Mount Edgar Dome (East Pilbara Terrane, Western Australia), modified after Gardiner et al. [33]. Yellow dots indicate sample locations.

scattered electron (BSE) detectors and are provided in Supplementary File 4.

U-Pb and Hf isotope analyses in zircon were performed by LA-MC-ICP-MS at the MILESTONE Laboratory (RéGEF ISOTOP-MTP, Geosciences Montpellier) using a Thermo Scientific Neptune XT multicollector inductively coupled plasma mass spectrometer (MC-ICP-MS) equipped with an optional multiple ion counters (MIC) package for U-Pb analysis. The MC-ICP-MS was coupled with a Teledyne Cetac Analyte Excite+ Excimer laser (193 nm) equipped with an optional X-Y Theta dynamic aperture allowing rectangular-shaped beams of any aspect ratio and orientation to be generated.

For U-Pb data acquisition, a low mass resolution mode was used to measure ^{202}Hg, ^{204}(Pb + Hg), ^{206}Pb, ^{207}Pb, ^{232}Th, and ^{238}U. Ion counters were used to measure m/z 207, 202, and 204, whereas Faraday cups were used to measure m/z 206, 232, and 238. Analyses were carried out using 15 s background measurements and a 25 s analysis with 400 cycles of 0.062 s each. Laser ablation was performed using a $12 \times 12\,\mu$m beam, a repetition rate of 4 Hz and an energy density of 4 J/cm^2. The data were reduced offline using the U-Pb geochronology data reduction scheme of the Iolite software [52–54]. A standard bracketing correction was performed, using the 91500 reference material (1065.4 ± 0.6 Ma [55]) as a primary standard. The data reduction included correction for the gas blank, laser-induced elemental fractionation of Pb and U, and instrumental mass bias. Corrections were interpolated using a linear spline function. Within-run ^{204}Pb was small (ca. <200 cps) compared to the m/z 204 background measurements (ca. 10-20 kcps), and no common Pb correction was applied. U-Pb ages were calculated using Isoplot R [56]. Secondary reference materials BB9 (562 ± 9 Ma; [57]), Plešovice (337.13 ± 0.37 Ma; [58]), and Kaap Valley (3229 ± 5 Ma; [59]) were analysed to monitor the accuracy of the data. The ages obtained with our approach are (within error) identical to the reference values, with BB9 = 563.6 ± 2.0 Ma, Plešovice = 337.6 ± 1.3 Ma, and Kaap Valley = 3225.2 ± 5.2 Ma. All errors are given at the 2σ level. The crystallisation ages of the samples were determined from the "least disturbed" analyses, i.e., for zircons with a high degree of concordance (relative difference between ^{207}Pb/^{206}Pb and ^{206}Pb/^{238}U ages between 95% and 105%) and for which a thorough inspection of within-run raw intensities suggests the absence of composite age domains or microinclusions not identified in SEM images (Supplementary File 4). The best estimate for the crystallisation age of each sample is given by the weighted mean average of ^{207}Pb/^{206}Pb ages.

Zircon Lu-Hf analyses were carried out using a 25×25 μm or $30 \times 30\,\mu$m beam, a laser frequency of 5 Hz and an energy density of 6 J/cm^2. Analyses were done on top of the U-Pb ablation pits. A typical analysis was 90 s, including a 30 s background measurement and a 60 s ablation period of

Table 1: A summary of key features for the Mount Edgar Dome granitoids selected for this study.

Sample No.	QAPF classification	Mineralogy	WGS84-south	WGS84-east	Grain size	Deformation
Callina Supersuite						
WA17-31	Granodiorite	Qz, Plg, Or, Ms+Chl, Zrn, Ttn, Ap, Ep, Ox	21°23′23.82″	120°11′27.78″	Medium	Nonfoliated
WA17-35	Monzogranite	Qz, Plg, Or, Bt+Ms+Chl, Zrn, Ap, All+Ep, Fl, Ox	21°10′04.23″	119°45′46.04″	Medium	Nonfoliated
Tambina Supersuite						
WA17-37	Tonalite	Qz, Plg, Or, Bt+Ms+Chl, Zr, Ap, All+Ep, Ox	21°18′06.11″	119°53′48.94″	Fine	Nonfoliated
Emu Pool Supersuite						
WA17-30	Tonalite	Qz, Plg, Or, Bt+Chl, Zrn, Ttn, Ap, Aln+Ep, Ox	21°00′19.25″	120°11′54.35″	Coarse	Nonfoliated
WA17-32	Tonalite	Qz, Plg, Or, Bt+Chl, Zrn, Ttn, Ap, Ep, Ox	21°16′03.20″	120°13′13.24″	Coarse	Nonfoliated
WA17-34	Tonalite	Qz, Plg, Or, Bt+Ms+Chl,Zrn, Ttn, Ap, Aln+Ep, Ox	21°11′42.86″	120°05′03.63″	Medium to coarse	Nonfoliated
WA17-36	Granodiorite	Qz, Plg, Or, Bt+Chl, Zrn, Ttn, Ap, Aln+Ep, Ox	21°13′48.29″	119°53′04.98″	Medium	Nonfoliated
WA17-27	Monzogranite	Qz, Plg, Or, Bt+Ms+Chl, Zr, Ti, Ap, Grt, Ep, Sil, Ox	21°08′38.77″	119°54′19.89″	Fine to medium	Nonfoliated
WA17-33	Granodiorite	Qz, Plg, Or, Bt+Chl, Zrn, Ttn, Ap, All+Ep, Ox	21°12′48.22″	120°15′37.87″	Medium to coarse	Nonfoliated
Cleland Supersuite						
WA17-28	Monzogranite	Qz, Plg, Or, Bt+Ms+Chl, Zrn, Ttn, Ap, All+Ep, Ox	21°04′07.58″	119°58′28.76″	Medium	Weakly foliated

60 cycles of 1 s each. 10 to 60 cycles were integrated for each measurement, depending on the stability of measured raw intensities. Correction for the interferences and mass bias was carried out using an in-house Excel spreadsheet. The correction for the isobaric interference of Yb and Lu on ^{176}Hf was made following a method initially set up at the Bristol Isotope Group (University of Bristol) and detailed in [60]. For Yb, the interference-free ^{171}Yb was corrected for mass bias effects using an exponential law and ^{173}Yb/^{171}Yb = 1.132685 [61]. The mass bias-corrected ^{171}Yb was monitored during the run and the magnitude of the ^{176}Yb interference on ^{176}Hf was calculated using ^{176}Yb/^{171}Yb = 0.901864 [61]. For Lu, the interference-free ^{175}Lu was corrected for mass bias effects assuming βLu = βYb and using an exponential law. The mass bias-corrected ^{176}Lu was monitored during the run, and the magnitude of the ^{176}Lu interference on ^{176}Hf was calculated using ^{176}Lu/^{175}Lu = 0.02655 [62]. Interference-corrected ^{176}Hf/^{177}Hf was corrected for mass bias using an exponential law and ^{179}Hf/^{177}Hf = 0.7325 [63] and were finally normalised to JMC – 475 = 0.282160. The accuracy and long-term reproducibility of the measurements were gauged by performing repeated analyses of three zircon reference standards: Mud Tank (^{176}Hf/^{177}Hf = 0.282502 ± 28, n = 48 at 25 × 25 μm beam; 0.282502 ± 18, n = 18 at 30 × 30 μm beam), Plešovice (^{176}Hf/^{177}Hf = 0.282480 ± 21, n = 45 at 25 × 25 μm beam; 0.282477 ± 17, n = 15 at 30 × 30 μm beam), and Temora-2 (0.282688 ± 36, n = 12 at 25 × 25 μm beam; 0.282693 ± 2 n = 6 at 30 × 30 μm beam). Our data are in agreement with the accepted ^{176}Hf/^{177}Hf ratios for Mud Tank (0.282504 ± 44; [64]), Plešovice (0.282482 ± 13; [58]), and Temora-2 (0.282680 ± 31; [65]). All errors are given at 2 s.d. level. ^{176}Hf/^{177}Hf initial ratios were calculated using the ^{176}Lu decay constant quoted in [66]. Only analyses with a precision better than 150 ppm (2 s.d.) were considered for this study. $\varepsilon Hf_{(t)}$ values were calculated using ^{176}Lu/^{177}Hf = 0.0336 and ^{176}Hf/^{177}Hf = 0.282785 for the CHUR [67].

4. Results

4.1. U-Pb Geochronology. 308 U-Pb analyses of zircons from 10 samples associated to four Supersuites across the Mount Edgar Dome (Figure 2, yellow dots) are reported in Supplementary Table 2. Wetherill Concordia diagrams and ^{207}Pb/^{206}Pb weighted mean ages for concordant to subconcordant zircons (i.e., analyses with 95 to 105% concordance) are shown in Figure 3. As a key information in this figure, upper intercept ages in Wetherill diagrams (Figure 3 (left panels)) and ^{207}Pb/^{206}Pb weighted mean ages (Figure 3 (right panels)) are identical within errors. Wetherill Concordia diagrams for the entire U-Pb data set that includes highly discordant analyses are provided in Supplementary File 4.

Zircons from the Callina Supersuite provide few concordant to subconcordant U-Pb ages (10 out of 54 analyses). The ^{207}Pb/^{206}Pb weighted mean ages for the most concordant data are 3465 ± 22 Ma and 3468 ± 13 Ma for samples WA17-31 and WA17-35, respectively (Figure 3(a)).

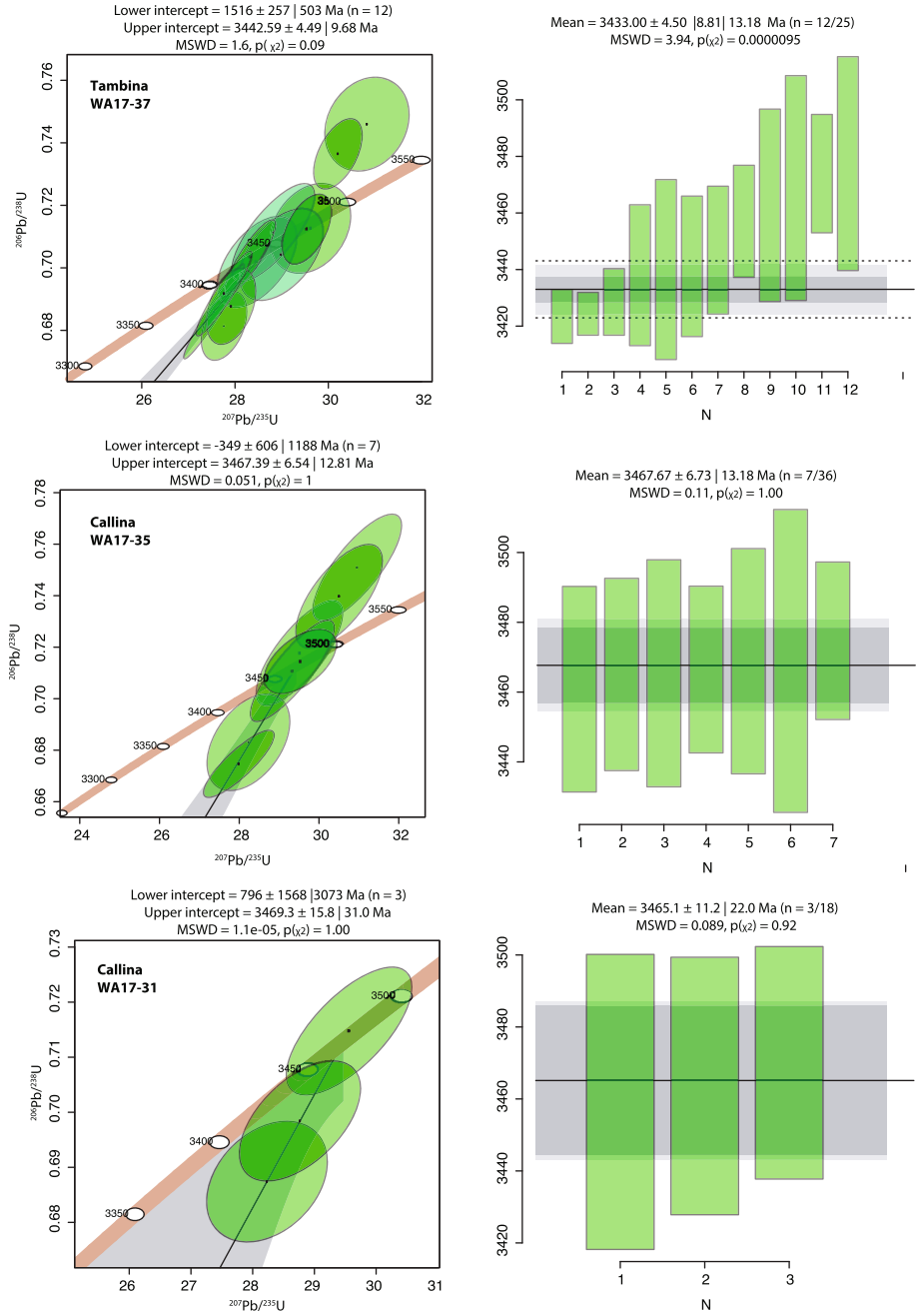

(a)

FIGURE 3: Continued.

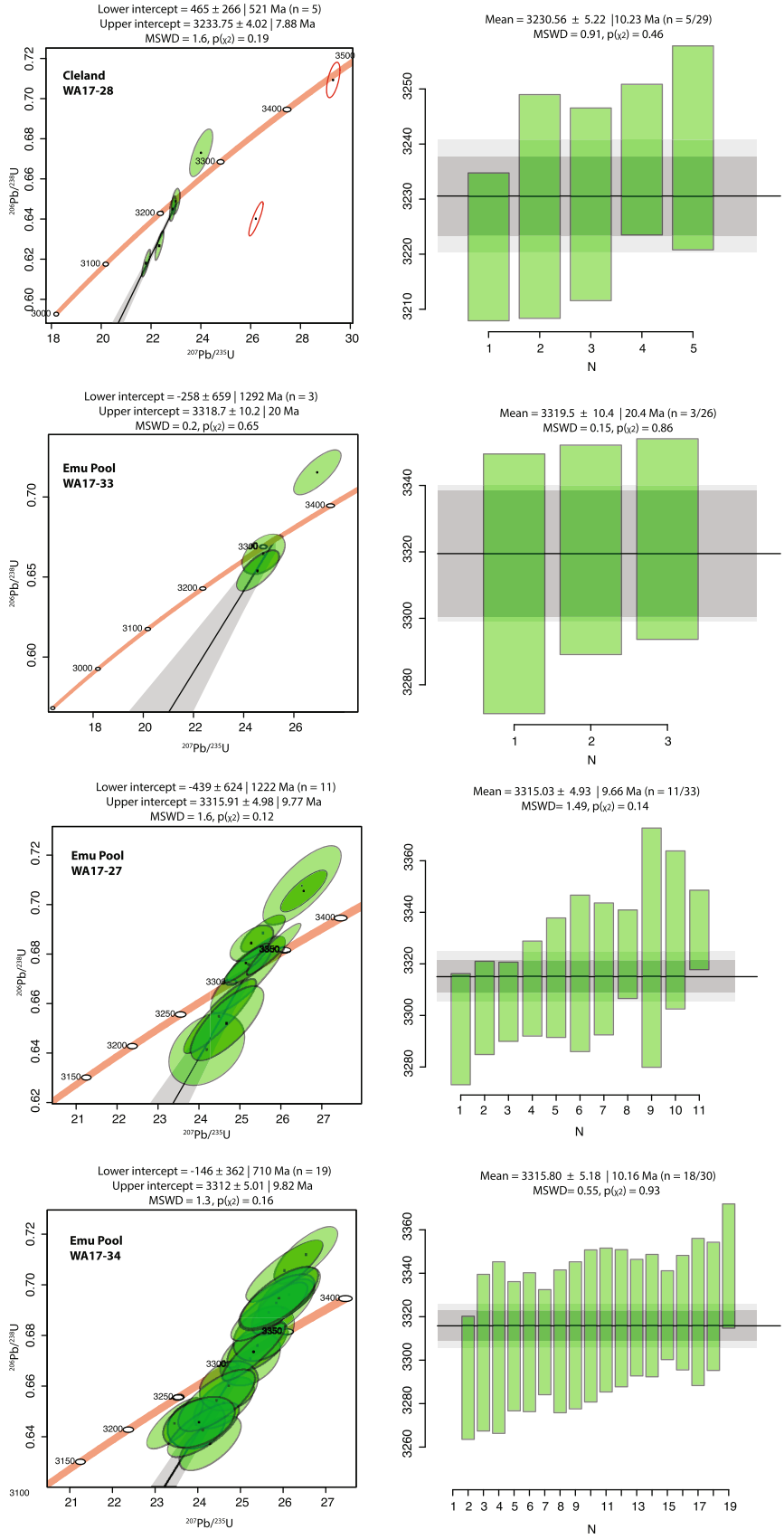

(b)

FIGURE 3: Continued.

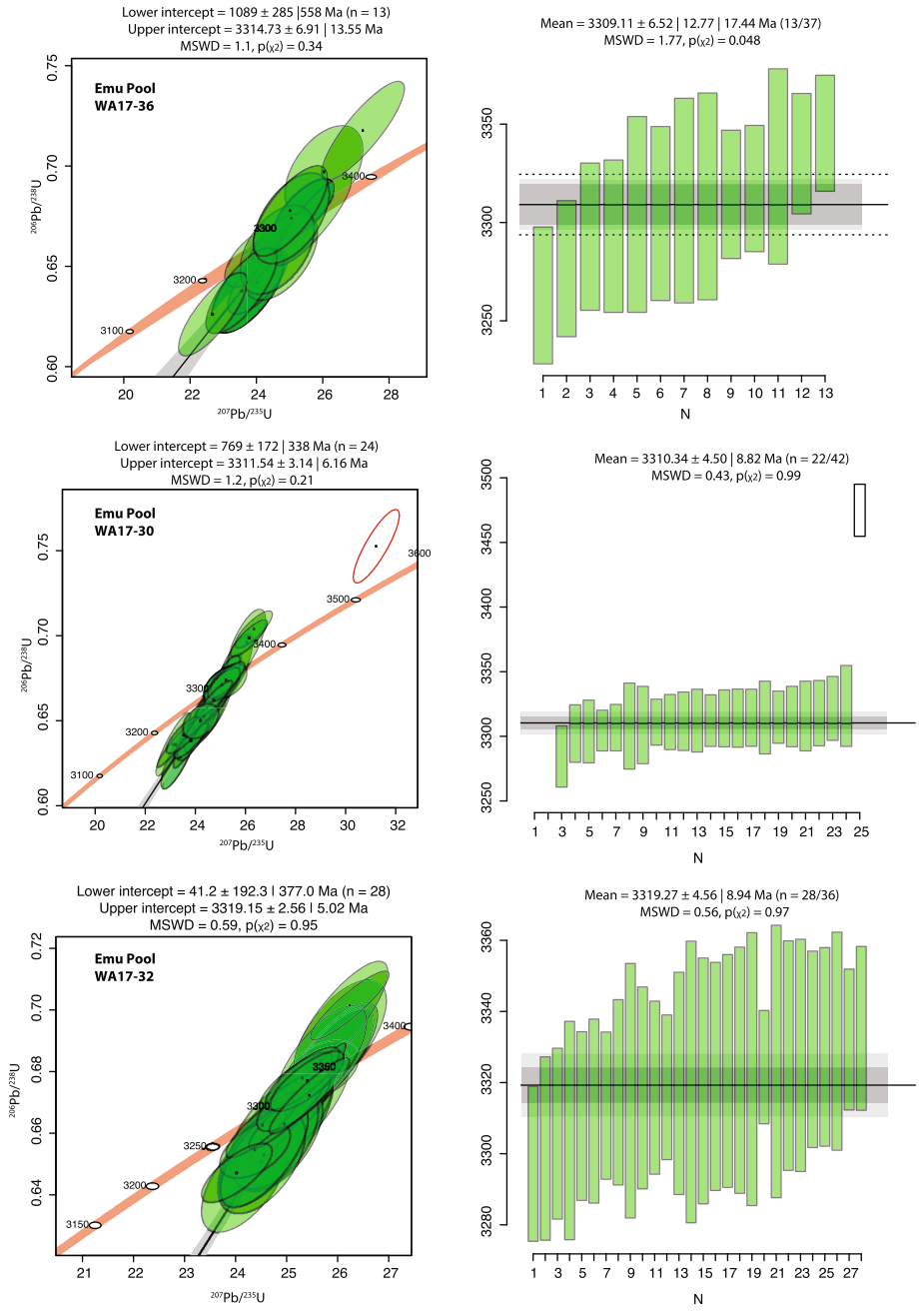

(c)

FIGURE 3: Summary of sub-concordant to concordant U-Pb analyses (by LA-MC-ICP-MS) of zircons from the Mount Edgar Dome. (a) Tambina and Callina Supersuites, (b) Emu Pool and Cleland Supersuites and (c) Emu Pool Supersuite. A laser ablation beam of only 12 $\times$ 12 μm allowed to obtain a high spatial resolution without compromising the precision and the accuracy of the data. For each sample, upper intercept ages (Wetherill Concordia diagrams on the left panel) and weighted mean $^{207}Pb/^{206}Pb$ ages (right panel) are identical within error. All errors are given at the 2σ level. Red empty ellipses are for inherited cores analyses.

The Tambina Supersuite zircons (sample WA17-37) generate a reasonable number of concordant to subconcordant U-Pb ages (12 out of 25 analyses), with a $^{207}Pb/^{206}Pb$ weighted mean age of 3433 ± 13 Ma (Figure 3(a)).

Zircons from the Emu Pool Supersuite provide a fair number of concordant to subconcordant U-Pb ages (103 out of 240 analyses), with $^{207}Pb/^{206}Pb$ weighted mean ages of 3309 ± 13 Ma (sample WA17-36), 3310 ± 9 Ma (WA17-30), 3316 ± 10 Ma (WA17-34), 3319 ± 20 Ma (WA17-33), 3315 ± 10 Ma (WA17-27), and 3319 ± 9 Ma (WA17-32). Sample WA17-30 has one zircon that shows an inherited core surrounded by a magmatic rim structure. One core analysis is concordant at 3469 ± 11 Ma, and two analyses performed on the rim gave younger concordant ages of 3304 ± 9 Ma and 3315 ± 15 Ma (Figures 3(b) and 3(c)).

The Cleland Supersuite zircons (WA17-28) generate a small number of concordant to subconcordant U-Pb ages (5 out of 26 analyses), with a $^{207}Pb/^{206}Pb$ weighted mean age of 3231 ± 10 Ma. Two grains with a well-defined core-and-rim structure could be identified and dated. One grain has a discordant core (analysis WA17-28-7c1, see Supplementary Table 2) for which the minimum crystallisation age is given by its $^{207}Pb/^{206}Pb$ age of 3480 ± 11 Ma and a concordant rim (WA17-28-7r1) with a $^{207}Pb/^{206}Pb$ age of 3257 ± 10 Ma. Another grain has an inherited core on which two analyses could be performed: one concordant analysis with a $^{207}Pb/^{206}Pb$ age of 3469 ± 10 Ma (WA17-28-10c2) and one discordant analysis with a $^{207}Pb/^{206}Pb$ age of 3455 ± 7 Ma (WA17-28-10c1). The rim analysis for this grain (WA17-28-10r1) is discordant, with a $^{207}Pb/^{206}Pb$ age of 3119 ± 11 Ma (Figure 3(b)).

Overall, the ages obtained here are in good agreement with the data published for the Callina, Tambina, Emu Pool, and Cleland Supersuites [28, 33, 34, 41, 68].

4.2. Major and Trace Elements. The major and trace element data for the Mount Edgar Dome granitoids are presented in Supplementary Table 1. The samples from the Callina and Tambina Supersuites show a narrow range of SiO_2 contents (73.0-76.5 wt%) and relatively low Al_2O_3 (12.8-14.0 wt%). They have high Na_2O (4.18-5.24 wt%), variable K_2O (1.70-3.80 wt%), low K_2O/Na_2O ratios (0.32-0.78), and variable Mg# (13-34 ($Mg\# = 100 \times mol\ MgO/[MgO + FeO_t]$)). They classify as metaluminous to slightly peraluminous with A/CNK ratios between 0.98 and 1.02.

Samples from the Emu Pool Supersuite are characterised by more scattered SiO_2 contents (66.9-75.2 wt%). They have variable concentrations of Al_2O_3 (13.5-16.0 wt%), MgO (0.15-1.31 wt%), CaO (0.90-3.46 wt%), and FeO_t (1.05-4.05 wt%) that correlate negatively with the SiO_2 content. The K_2O and Na_2O contents show limited variations (1.70-2.76 wt% and 4.54-5.25 wt%, respectively), and K_2O/Na_2O ratios are low (0.26-0.61), except for one sample that has higher K_2O (4.54 wt%), lower Na_2O (3.84 wt%), and a K_2O/Na_2O ratio of 1.18. All samples classify as metaluminous to slightly peraluminous with a A/CNK ratio between 0.97 and 1.04, and their Mg# shows a wide range of variation between 18 and 40.

The sample from the Cleland Supersuite has a high SiO_2 content (72.2 wt%), although other major elements fall within the range of values of the Emu Pool Supersuite: Na_2O = 3.96 wt%, Al_2O_3 = 14.2 wt%, MgO = 0.45 wt%, CaO = 1.92 wt%, FeO_t = 14.2 wt%, and K_2O = 3.77 wt%. It classifies as slightly peraluminous and has a Mg# of 29.

In the normative Ab-An-Or diagram, the Mount Edgar Dome granitoids plot in the tonalite, trondhjemite, and granite fields (Figure 4(a)). In the classification diagram of Laurent et al. [69] for Archaean granitoids, they plot in the "TTG" and "biotite and two-mica granites" fields (Figure 4(b)). The SiO_2 content ranges from 66 to 75 wt% (with samples that can be classified as TTGs having lower SiO_2), and a negative correlation with the Mg# is observed (Figure 4(c)). Samples that plot in the granite fields in Figures 4(a) and 4(b) have higher K_2O and lower Na_2O, CaO, Fe_2O_3, and Al_2O_3 contents than samples that plot in the TTG fields (Supplementary File 3). The samples classified as TTGs also have low K_2O/Na_2O (<0.5), and samples from both TTG and granite groups straddle between the metaluminous and peraluminous fields in Figure 4(d). Finally, samples with a higher aluminium saturation index are more enriched in SiO_2 irrespective of the classification group (Figures 4(c) and 4(d)).

The trace element data reveal low concentrations in compatible elements, especially for Cr and Ni (<20 ppm) and V (<40 ppm). For incompatible elements, Ba and Sr are below 600 and 1000 ppm, respectively. The sample from the Cleland Supersuite (WA17-28) has a much higher Sr content (~1300 ppm), which appears to be an exception. All samples show a broad negative slope in a primitive mantle-normalised trace element diagram, and the granite group has a distinct negative Sr anomaly that is absent in the TTG group (Supplementary Figure 2). One sample from the Emu Pool Supersuite (WA17-27) is remarkably enriched in Rb (430 ppm), Th (33 ppm), and U (12 ppm). It has high HREE contents and a negative Eu anomaly, and the presence of muscovite and aluminosilicates in its paragenesis makes it similar to crustal melts such as Himalayan leucogranites [70].

The initial division into two groups, i.e., granites and TTGs, is substantiated by trace element analyses. Samples belonging to the granite group show more fractionated trace element patterns with flat HREE, negative Nb, Ta, Sr, Zn, and Eu anomalies, and enriched trace elements contents (Figure 4(f) and Supplementary File 3). The sample from the Cleland Supersuite (WA17-28) has an intermediate composition between the granite and TTG groups. It has a steep HREE pattern with a high $(La/Yb)_N$ ratio commonly observed in TTGs, but it also has a pronounced negative Eu anomaly and a high K_2O/Na_2O ratio (>0.9), which is a typical common feature of granites. It is therefore included in the granite group here. Overall, the granite group defined in this study differs from the high-HREE TTG group of Halla et al. [71], because it presents a 10-times HREE enrichment compared to the chondrites and has a strong negative Eu anomaly, which are not common features in high-HREE TTGs.

The samples belonging to the TTG field are less enriched in trace elements, and they show no Eu and Sr anomalies and have slightly positive Hf anomalies (Figure 4(f) and Supplementary File 3). They show higher $(La/Yb)_N$ and Sr/Y ratios than the granite group (Figure 4(e)), they have enriched LREE relative to HREE and display steep HREEs in chondrite normalised REE patterns (Figure 4(f)).

4.3. Lu-Hf Isotopes. The initial $^{176}Hf/^{177}Hf$ ratios of zircons from the Mount Edgar Dome are plotted against $^{207}Pb/^{206}Pb$ ages in Figure 5, and the full Lu-Hf dataset is reported in Supplementary Table 2. When zircons with both concordant and discordant U-Pb ages are considered, they define subhorizontal trends that are typical of lead losses (Figure 5).

To overcome Pb loss issues when interpreting data, initial $^{176}Hf/^{177}Hf$ ratios were calculated using the best estimate for the crystallisation age of each sample, which is given by the $^{207}Pb/^{206}Pb$ weighted mean ages calculated in Figure 3.

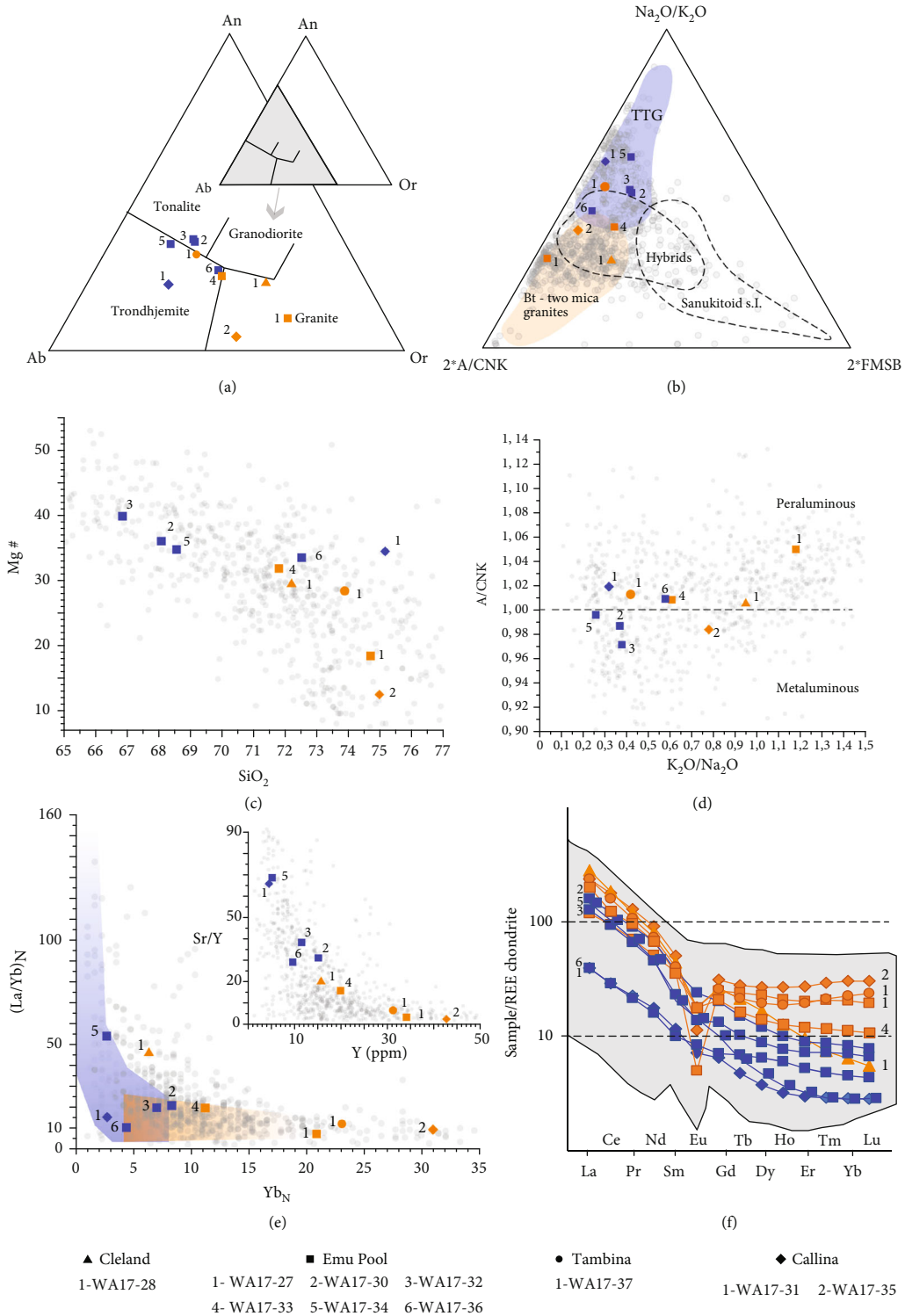

FIGURE 4: Classification diagrams for the Mount Edgar Dome granitoids based on (a) their normative Albite (Ab)-Anorthite (An)-Orthoclase (Or) composition (after Barker [72]), (b) the classification of Laurent et al. [69] for Archaean granitoids, (c) a plot of SiO_2 vs. Mg#, (d) a plot of K_2O/Na_2O vs A/CNK, (e) plots of La/Yb_N vs. Yb_N and Sr/Y vs. Y, and (f) chondrite normalised REE patterns. Grey data points in (b–e) and grey field in (f) are literature data of [73] for granitoids from the East Pilbara Terrane.

A summary of the mean $^{207}Pb/^{206}Pb$ ages and the Lu-Hf isotope composition of the 10 samples selected for this study is given in Table 2.

The two samples from the Callina Supersuite have superchondritic mean $\varepsilon Hf_{(t)}$ of $+1.7 \pm 0.7$ (WA17-31) and $+1.5 \pm 0.5$ (WA17-35) (2 s.e.). The sample from the Tambina

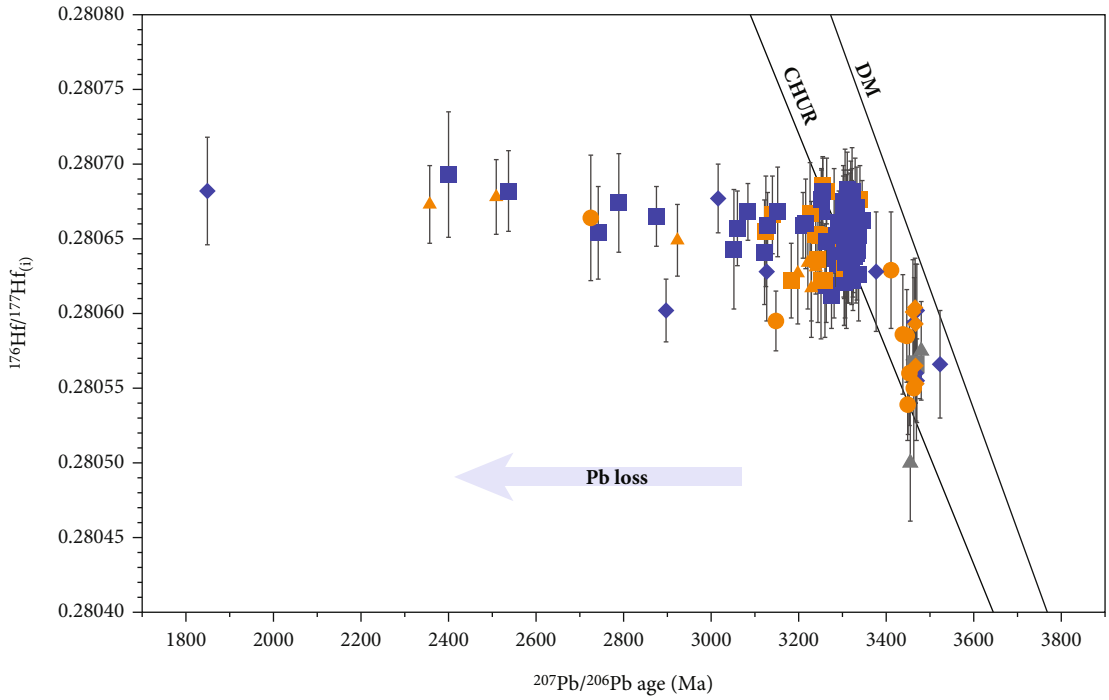

FIGURE 5: Initial Hf isotope composition as a function of the $^{207}Pb/^{206}Pb$ age of zircons from the Mount Edgar Dome. Blue and orange symbols are for the TTG group and the granite group, respectively (see Figure 4). Diamonds: Callina Supersuite; circles: Tambina Supersuite; squares: Emu Pool Supersuite; triangles: Cleland Supersuite.

Supersuite (WA17-37) shows a mean $\varepsilon Hf_{(t)}$ that is chondritic within error (+0.5 ± 0.7). The six samples from the Emu Pool Supersuite define a limited range of $\varepsilon Hf_{(t)}$ variation, from +0.1 ± 0.5 to +0.8 ± 0.4 (WA17-33: +0.1 ± 0.5, WA17-32: +0.3 ± 0.3, WA17-30: +0.4 ± 0.3, WA17-36: + 0.4 ± 0.4, WA17-34: +0.7 ± 0.4, and WA17-37: +0.8 ± 0.4). In this Supersuite, one zircon with an inherited core dated at 3467 ± 7 Ma has a slightly superchondritic $\varepsilon Hf_{(t)}$ of +1.0 ± 0.9 (Supplementary Table 2). The Sample from the Cleland Supersuite displays a subchondritic mean $\varepsilon Hf_{(t)}$ of -1.9 ± 0.6 (Table 2), and one zircon with a slightly discordant inherited core dated at 3480 ± 11 Ma has a superchondritic $\varepsilon Hf_{(t)}$ of +1.6 ± 1.2.

5. Discussion

5.1. Petrogenesis of Ancient Granitic Rocks. The U-Pb data suggest that there is no clear temporal correlation between samples classified as TTGs and granites, and both magma types were formed coevally in at least two different periods, ~3.47 and ~3.32-3.31 Ga. The potential magmatic sources for the Mount Edgar Dome granitoids can be inferred from the ternary plot in Figure 6. It suggests that the TTG group may originate from a low-K mafic source, while the granite group plots between a low-K mafic source and a more differentiated tonalitic source.

At the source, given the stability of restite/peritectic minerals, magmas become depleted in elements preferentially retained in the restite. The HREE depletion of evolved TTG may indicate the presence of garnet as a residual phase and the absence of Eu anomaly suggests that plagioclase was not present, and thus that depths of magma generation may have occurred beyond 12 kbar [8]. Although the $(La/Yb)_N$ and Sr/Y ratios have been widely used to infer depths of magma extraction, they could also be modified by amphibole fractionation and plagioclase accumulation of the same parental magma extracted at depth [74]. Thus, garnet as a residual phase may not be necessary to explain the geochemical signature observed, and magmatic evolution of the TTG group could have occurred at relatively shallower levels [74]. In contrast, the granite group originated at shallow levels due to pronounced Eu and Sr negative anomalies and higher enrichment in HREE compared to the TTG group.

Once ascending within the crust, magmas progressively become more differentiated due to fractional crystallisation (e.g., [75]). Nonetheless, a direct extraction from a mantle source followed by intense fractional crystallisation is unlikely to have produced large volumes of evolved magmas, because it would require a low degree of partial melting in the Archaean, when geothermal conditions were higher [76]. A two-stage formation that involves extraction of a basaltic source from the mantle and further remelting is more compatible with both experimental models and the thermal conditions in the early Earth [76]. Moreover, both TTG and granite groups in the MED show evidence for intense crustal reworking, such as very high SiO_2 contents, low Mg#, and low contents in compatible elements (e.g., Ni, Cr, and V). The geochemistry of the studied rocks suggests that the granitoid magmas did not interact or were in equilibrium with mantle material directly (e.g., [77]); instead

Table 2: Summary of the mean crystallisation age and the Lu-Hf isotope composition of zircons from Mount Edgar Dome granitoids.

Sample No.	Rock type	$^{207}Pb/^{206}Pb$ zircon age (Ma)	2σ	$^{176}Lu/^{177}Hf$	$\varepsilon Hf_{(t)}$	2 s.e.	$^{176}Hf/^{177}Hf$	$^{176}Hf/^{177}Hf_{(i)}$	2 s.e.	Number of Hf analyses
Tonalites and Thronjemites										
Callina Supersuite										
WA17-31	Trondhjemite	3465	22	0.0017	1.7	0.7	0.280713	0.280588	0.000019	10
Emu Pool Supersuite										
WA17-30	Tonalite	3310	9	0.00084	0.4	0.3	0.280704	0.280654	0.000009	24
WA17-32	Tonalite	3319	9	0.00057	0.3	0.3	0.280681	0.280644	0.000009	21
WA17-34	Trondhjemite	3316	10	0.00072	0.7	0.4	0.280706	0.280659	0.000010	19
WA17-36	Trondhjemite	3309	17	0.00137	0.4	0.4	0.280742	0.280656	0.000012	18
Granites										
Callina Supersuite										
WA17-35	Granite	3468	13	0.00258	1.5	0.5	0.280745	0.280581	0.000014	5
Tambina Supersuite										
WA17-37	Granite	3433	13	0.00183	0.5	0.7	0.280694	0.280574	0.000020	7
Emu Pool Supersuite										
WA17-27	Granite	3315	10	0.00093	0.8	0.4	0.280719	0.280663	0.000012	11
WA17-33	Granite	3320	20	0.0011	0.1	0.5	0.280703	0.280640	0.000015	11
Cleland Supersuite										
WA17-28	Granite	3231	10	0.00096	-1.9	0.6	0.280689	0.280642	0.000017	9

they would be the product of intracrustal reworking at different levels of the crust with different stages of differentiation and fractional crystallisation (e.g., [78]).

The generation of TTG magmas is inferred to have occurred via partial melting of altered basalt followed by fractional crystallisation, whereas granites were generated from a different process. Samples from the granite group show relatively more evolved geochemical signatures, which include a pronounced negative Eu anomaly, an enrichment in the most incompatible elements, higher SiO_2 and lower Mg#, and yet further enrichment in K_2O and LILE. Experimental models have demonstrated that an extra component is needed to explain the enrichment in LILE and K_2O, which can derive from the alteration of a basaltic source or from an enrichment in continental crust-derived components [46]. Although samples from the granite group may have been formed close to the granitic minimum, i.e., without fractional crystallisation [79], their generation might have involved, at least to a small extent, mixing between a product of remelting of older TTG rocks and a primary TTG melt from a basaltic source (e.g., [80]). Therefore, we posit that this group results from a more complex petrogenesis than fractional crystallisation or partial melting of a TTG end-member alone (e.g., [77]). One hypothesis is that mafic source(s), similar to those from which TTG magmas derived, have melted and combined with partial melting products of reworked TTGs. The mixture between an original TTG melt and a remelting product of an existing TTG would then form the granite-like compositions [77]. This is consistent with the presence of inherited zircons in granitoids that crystallised at ~2.8 and ~3.3 Ga [33, 34].

The enrichment in REE, LILE, and the negative Eu anomaly suggests that the granite group is geochemically similar to post-Archaean occurrences of the BADR (Basalt-Andesite-Dacite-Rhyolite) magmatic series. This geochemical signature is not related to post-Archaean secondary processes; it rather demonstrates that Palaeoarchaean tectonics were capable of producing highly evolved magmas akin to younger granites in the absence of modern-style plate tectonics. The generation of TTG and more evolved granitic magmas may have occurred in intraplate stagnant lid settings as well as in hot subduction environments, since both tectonic settings can produce evolved magmas by partial melting and fractional crystallisation [6].

5.2. Chondritic or Depleted Mantle Source for the Mount Edgar Dome Granitoids. A number of models for the Archaean evolution of the Pilbara crust have been published, yet no consensus was reached on whether the mantle source of Pilbara granitoids was chondritic [26, 27, 32] or more depleted [33, 34]. Our zircon Hf isotope data has potential to bring new perspectives to the current debate, and a summary plot that includes literature data is given in Figure 7.

Petersson et al. [26, 32] and Salerno et al. [27] argued, based on isotopic analyses of accessory minerals and whole-rock compositions, that there is no evidence of a strongly depleted mantle source, or of mixing between different sources, in the generation of the granites from the EPT from 3.5 to 3.2 Ga. Petersson et al. [26] interpreted zircon Hf isotope signatures as successive juvenile additions to the crust from a "near-chondritic" reservoir ranging from -1.9 to +1.9 in the εHf space, and they suggested that the large range of εHf variation of this reservoir could be explained by the uncertainty over the measurement of Lu-Hf isotopes by LA-MC-ICP-MS techniques. In addition,

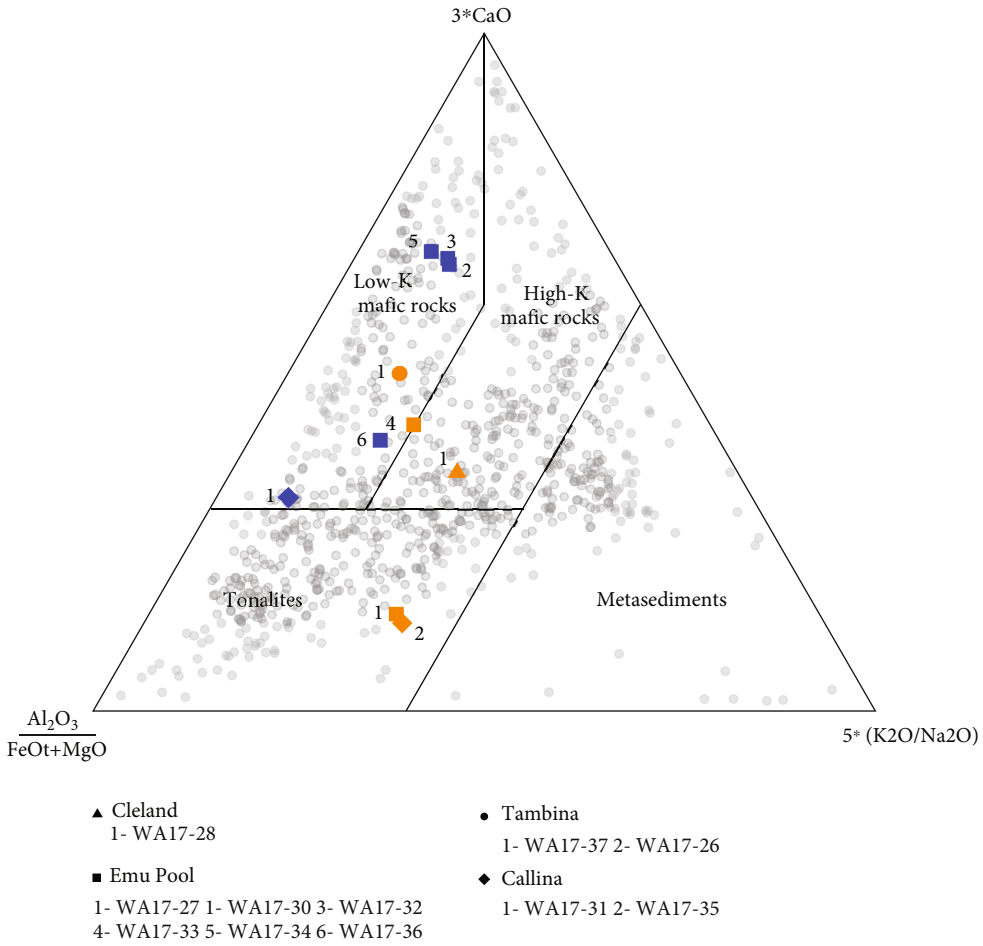

FIGURE 6: Ternary diagram of Laurent et al. [69] for the Mont Edgar Dome granitoids investigated in this study. This diagram shows the fields of compositions of melts derived from a range of potential sources determined from experimental studies. Blue and orange symbols are for the TTG group and the granite group, respectively (see Figure 4). Grey symbols are literature data of Hawksworth and Kemp [73] for granitoids from the East Pilbara Terrane.

Salerno et al. [27] argued that variations beyond chondritic values are artefacts of postcrystallisation alteration processes that occurred at the mineral scale.

In contrast, Gardiner et al. [33, 34, 81] offered an alternative interpretation where the earliest continental crust in the Pilbara area was extracted from a depleted mantle reservoir between 3.7 and 3.5 Ga. In their model, the Palaeoarchaean Supersuites of the Mount Edgar Dome derived partly from this ancient reservoir through intracrustal remelting and partly from minor juvenile additions at the time of magma crystallisation. This is in line with earlier studies ([30], e.g., [46, 82]) that recognized the presence of an older continental substrate under the domes of the East Pilbara Terrane, based on REE signatures and Hf-Nd isotope variations. Remnants of an old sialic crust are also inferred from 3.7 to 3.56 Ga Nd model ages [34, 83] and from the detrital zircon record in which crystallisation ages ranging 3.8-3.53 Ga were identified [44, 49, 84].

In Figure 7, three distinct groups of samples with a narrow range of Hf isotope compositions can be identified from our data: (i) a superchondritic group at 3.47 Ga, with a mean $\varepsilon Hf_{(t)} = 1.6 \pm 0.2$ (2 s.e); (ii) a chondritic to slightly superchondritic group at 3.43 Ga (mean $\varepsilon Hf_{(t)} = 0.5 \pm 0.7$) and 3.32-3.31 Ga (mean $\varepsilon Hf_{(t)} = 0.45 \pm 0.2$) and later referred to as "near-chondritic group"; and (iii) a subchondritic group at 3.23 Ga (mean $\varepsilon Hf_{(t)} = -1.9 \pm 0.6$). The origin and the significance of these three groups are discussed below.

The presence of a superchondritic group at 3.47 Ga advocates for a depleted mantle reservoir in the Pilbara area at ca. 3.5 Ga. This reservoir would have separated from the chondritic mantle before 3.8 Ga (Figure 7), which is consistent with older (>3.5 Ga) continental material in Pilbara testified by tonalite and metagabbros dated between 3.65 and 3.58 Ga (e.g., [32, 35]), inherited zircons in igneous rocks and detrital zircons with crystallisation ages ranging between 3.5 and 3.7 Ga [20–22, 44, 83, 84], and $T_{(DM)}$ model ages calculated from the bulk-rock Sm-Nd and Lu-Hf isotope data ranging 3.8-3.5 Ga [21, 22, 52, 84].

The near-chondritic group contains one granite at 3.43 Ga and both TTGs and granites at 3.31-3.32 Ga. The presence of granitoids in Pilbara with chondritic signatures may be explained in three different ways: (i) a direct origin

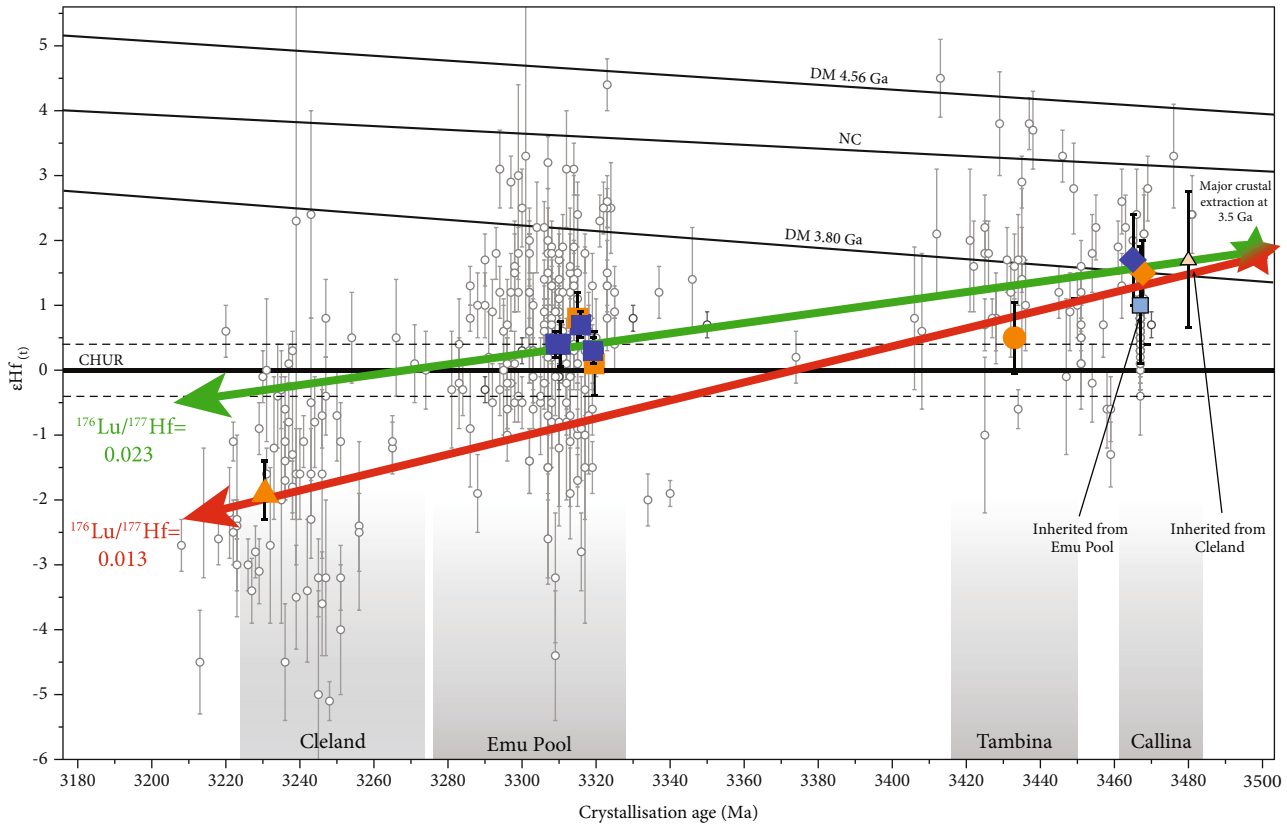

FIGURE 7: A plot of $\varepsilon Hf_{(t)}$ versus crystallisation age for zircons from the Mount Edgar Dome granitoids. Coloured symbols are for this work and grey symbols are for literature data [27, 32, 34, 78]. Blue and orange symbols are for the TTG group and the granite group, respectively (see Figure 4). Smaller coloured symbols represent analyses of inherited cores. The two "DM" lines represent the evolution of the depleted mantle that separated from a chondritic mantle either at 4.56 Ga or at 3.8 Ga (e.g., [25]), and with a present-day εHf = +17 [81]: NC: new crust evolution line from Ref. [82].

from a chondritic reservoir, through remelting of a mafic protolith soon after its extraction from the chondritic mantle; (ii) mixing between the superchondritic depleted mantle and some subchondritic ancient crust, in proportions that fortuitously resulted in near-chondritic Hf isotope signatures; or (iii) the protracted reworking of a crustal source with which the 3.47 Ga superchondritic group shares a common origin.

We posit that the absence of any "mixing trend" in our data, which should be evidenced by the vertical scattering of our samples between superchondritic and subchondritic $\varepsilon Hf_{(t)}$ signatures in Figure 7, along with the likely slow mantle homogenisation during the Palaeoarchaean [85] reasonably exclude the hypothesis of mixed mantle and crustal reservoirs in the source of the near-chondritic group. The presence of inherited zircons in the granitoids from this group ([34]; this study), for which the crystallisation ages and the Hf isotope compositions are similar to those of the superchondritic group (e.g., light blue square in Figure 7), challenges a pure mantle origin for the near-chondritic group and favours a model involving the protracted remelting of an ancient crustal source.

The subchondritic group is defined by one granite that crystallised at 3.32 Ga. Likewise the near-chondritic group, granitoids contain inherited zircons with crystallisation ages and Hf isotope compositions similar to those of the superchondritic group ([34]; this study). Overall, ubiquitous inherited zircons with ages ~3.46-3.48 Ga in the Mount Edgar Dome granitoids suggest that the reworking of crustal source(s) was a major process involved in the evolution of the Pilbara crust through time.

5.3. Palaeoarchaean Crustal Evolution in Pilbara. In Pilbara, the presence of a protocratonic crust has been evidenced as far back as 3.80 Ga [34, 83], and the processes involved in the formation of this crust remain debated. A shift towards more juvenile Hf isotope signatures in zircon was recently evidenced between 3.8 Ga and 3.6 Ga in a number of cratons worldwide, and it was interpreted by a change in geodynamic style from vertical to mobile lid tectonics [85, 86]. However, there is little evidence of robust, highly negative εHf data in the Pilbara Craton for that time period [32], and the oldest "undisturbed" zircons in Pilbara (ca. 3.7 Ga) have near-chondritic εHf values [83].

One striking feature in Figure 7 is that our samples define two crustal evolution trends. The first trend, constrained by the Callina and Emu Pool granitoids, has a calculated $^{176}Lu/^{177}Hf$ ratio (slope) of 0.023 that is typical of the

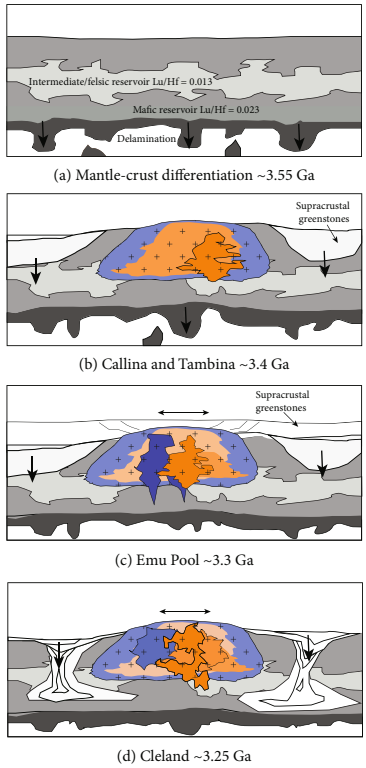

FIGURE 8: Illustration of the crustal evolution of the Pilbara area in the period 3.5–3.25 Ga. (a) Initial conditions: mantle–crust differentiation event and formation of two crustal reservoirs with different Lu/Hf ratios. (b) Formation of Callina TTGs and granites from both mafic and intermediate/felsic reservoirs, followed by the formation of Tambina granites from the intermediate/felsic reservoir. (c) Formation of Emu Pool TTGs and granites from the mafic reservoir. (d) Formation of Cleland granites from the intermediate/felsic reservoir. Based on the model of Wiemer et al. [35].

time-integrated evolution of a mafic source. The second trend, constrained by the Callina, Tambina, and Cleland granitoids, has a calculated $^{176}Lu/^{177}Hf$ ratio of 0.013 that suggests a source of intermediate/felsic composition. These two trends converge at $t = 3.50$ Ga and $\varepsilon Hf_{(t)} = +2$, which suggests that a major crust differentiation event from a depleted mantle source occurred at ca. 3.50 Ga in the Pilbara area.

Our preferred interpretation for the Palaeoarchaean evolution of the EPT is summarised in Figure 8. It shows the stages of partial convective overturn of middle and upper crust and generation of the dome-and-keel structure based on Refs. [35, 45]. At ca. 3.50 Ga, two distinct crustal reservoirs were generated from the melting of a depleted mantle source ($\varepsilon Hf_{(3.50\,Ga)} = +2$): (i) a mafic crust with $^{176}Lu/^{177}Hf = 0.023$ and (ii) an intermediate/felsic crust with $^{176}Lu/^{177}Hf = 0.013$ (Figure 8(a)). 3.47 Ga marks the onset of intracrustal reworking of these two reservoirs, associated with the formation of both TTGs and granites from the Callina Supersuite. At 3.43 Ga, the intermediate/felsic reservoir melted to produce granitic magmas from Tambina Supersuite (Figure 8(b)), with no evidence from our samples for a contribution of the mafic reservoir at this time. At 3.31 Ga the mafic reservoir melted to produce both TTGs and granites from the Emu Pool Supersuite, with no evidence for a contribution of the intermediate/felsic reservoir during this event (Figure 8(c)). The magmas that formed interacted with the 3.47 Ga crust of the Callina Supersuite, as evidenced from the presence of inherited zircons in Emu Pool granitoids. Finally, the intermediate/felsic crust reservoir was reworked at 3.25 Ga to produce granitic magmas from Cleland Supersuite. The presence in Cleland granites of inherited zircons contemporaneous with the timing of emplacement of the Callina Supersuite (Figure 8(d)) indicates the contribution of Callina-derived ancient crustal material in their source.

The absence of any "vertical spread" defined by our samples in the $\varepsilon Hf_{(t)}$ versus crystallisation age plot (Figure 7) suggests that after their formation at ca. 3.50 Ga, the mafic and intermediate/felsic crustal reservoirs remained isotopically isolated from each other and from the mantle for at least 200 Ma. One possible implication is that mobile lid tectonics was not a global process during the Eo/Palaeoarchaean and that vertical tectonics remained predominant in the Pilbara area [87]. The tectonic settings of crustal evolution started to change only after 3.2 Ga, when signs of lateral movements that lead to the ceasing of the diapiric doming start to appear in the EPT [36, 88].

6. Conclusions

Based on distinct geochemical characteristics, Palaeoarchaean granitoids from the Mount Edgar Dome can be separated into two groups. The first group has chondrite-normalised REE patterns and trace element compositions akin to TTGs. It represents highly fractionated magmas formed by partial melting of a basaltic source and extensive fractional crystallisation. The second group is slightly more enriched in incompatible elements and shares similar trace element features to post-Archaean granites. Beyond the differentiation of a primary TTG magma from the melting of a mafic crust, this group requires an extra component in its formation, such as the incorporation of melts derived from former TTG rocks. Both groups overlap in time and space without any clear temporal trend in their chemistry.

New, high-spatial resolution Hf isotope analyses indicate that for ~3.50 Ga, there was a major mantle–crust differentiation event, which led to the formation of two separate crustal reservoirs of mafic and intermediate/felsic compositions, respectively. The superchondritic isotope composition of these two reservoirs at 3.50 Ga ($\varepsilon Hf = +2$) points towards the presence of a depleted mantle in Pilbara at 3.5 Ga, which was separated from a chondritic reservoir prior to 3.8 Ga. Both crustal reservoirs have remained isolated from any new crustal or mantle input over at least ~200 Myr since 3.50 Ga. Protracted intracrustal remelting processes and differentiation have played a key role in the evolution of the Pilbara crust in the Palaeoarchaean, and the approach developed in this study opens new perspectives to better constrain the formation, evolution, and maturation of the building blocks of continents.

Data Availability

All data are available in the manuscript and supplementary material.

Conflicts of Interest

The authors declare that there are no conflicts of interest.

Acknowledgments

This project was funded by the European Research Council under the European Union's Horizon 2020 research and innovation program (No. 817934). The fieldwork in 2017 was supported by the Leverhulme Trust (grant RPG-2015–422). Christophe Nevado and Doriane Delmas made all thin sections for this study. Cyprien Astoury helped with samples crushing and heavy mineral separation. Frederic Fernandez helped with the acquisition of the zircon images through SEM.

Supplementary Materials

Supplementary 1. Supplementary Table 1: major and trace element data.

Supplementary 2. Supplementary Table 2: geochronological and Lu-Hf data.

Supplementary 3. Supplementary File 3: Harker, TAS, K_2O vs. Silica diagrams and trace element pattern plots.

Supplementary 4. Supplementary File 4: petrographic descriptions, thin section photographs, CL images of zircons analysed, and Wetherill diagrams.

References

[1] S. A. Bowring and I. S. Williams, "Priscoan (4.00-4.03 Ga) orthogneisses from northwestern Canada," *Contributions to Mineralogy and Petrology*, vol. 134, no. 1, pp. 3–16, 1999.

[2] S. A. Wilde, J. W. Valley, W. H. Peck, and C. M. Graham, "Evidence from detrital zircons for the existence of continental crust and oceans on the Earth 4.4 Gyr ago," *Nature*, vol. 409, no. 6817, pp. 175–178, 2001.

[3] S. J. Mojzsis, T. M. Harrison, and R. T. Pidgeon, "Oxygen-isotope evidence from ancient zircons for liquid water at the Earth's surface 4,300 Myr ago," *Nature*, vol. 409, no. 6817, pp. 178–181, 2001.

[4] A. I. S. Kemp, S. A. Wilde, C. J. Hawkesworth et al., "Hadean crustal evolution revisited: new constraints from Pb–Hf isotope systematics of the Jack Hills zircons," *Earth and Planetary Science Letters*, vol. 296, no. 1–2, pp. 45–56, 2010.

[5] J. D. Vervoort and J. Blichert-Toft, "Evolution of the depleted mantle: Hf isotope evidence from juvenile rocks through time," *Geochimica et Cosmochimica Acta*, vol. 63, no. 3–4, pp. 533–556, 1999.

[6] J.-F. Moyen and H. Martin, "Forty years of TTG research," *Lithos*, vol. 148, pp. 312–336, 2012.

[7] K. C. Condie, A. Davaille, R. C. Aster, and N. Arndt, "Upstairs-downstairs: supercontinents and large igneous provinces, are they related?," *International Geology Review*, vol. 57, no. 11–12, pp. 1341–1348, 2015.

[8] J.-F. Moyen, "The composite Archaean grey gneisses: petrological significance, and evidence for a non-unique tectonic setting for Archaean crustal growth," *Lithos*, vol. 123, no. 1–4, pp. 21–36, 2011.

[9] J.-F. Moyen, "Archean granitoids: classification, petrology, geochemistry and origin," *Geological Society of London, Special Publication*, vol. 489, no. 1, pp. 15–49, 2020.

[10] K. C. Condie, *Archean greenstone belts*, Elsevier, 1981.

[11] M. J. Van Kranendonk, W. J. Collins, A. Hickman, and M. J. Pawley, "Critical tests of vertical vs. horizontal tectonic models for the Archaean East Pilbara Granite–Greenstone Terrane, Pilbara Craton, Western Australia," *Precambrian Research*, vol. 131, no. 3–4, pp. 173–211, 2004.

[12] C. François, P. Philippot, P. Rey, and D. Rubatto, "Burial and exhumation during Archean sagduction in the East Pilbara Granite-Greenstone Terrane," *Earth and Planetary Science Letters*, vol. 396, pp. 235–251, 2014.

[13] R. M. Palin, M. Santosh, W. Cao, S.-S. Li, D. Hernández-Uribe, and A. Parsons, "Secular change and the onset of plate tectonics on Earth," *Earth Science Reviews*, vol. 207, p. 103172, 2020.

[14] B. Dhuime, A. Wuestefeld, and C. J. Hawkesworth, "Emergence of modern continental crust about 3 billion years ago," *Nature Geoscience*, vol. 8, no. 7, pp. 552–555, 2015.

[15] B. Dhuime, C. Hawkesworth, and P. Cawood, "When continents formed," *Science*, vol. 331, no. 6014, pp. 154-155, 2011.

[16] M. J. Van Kranendonk, "Onset of plate tectonics," *Science*, vol. 333, no. 6041, pp. 413-414, 2011.

[17] E. A. Belousova, Y. A. Kostitsyn, W. L. Griffin, G. C. Begg, S. Y. O'Reilly, and N. J. Pearson, "The growth of the continental crust: constraints from zircon Hf-isotope data," *Lithos*, vol. 119, no. 3–4, pp. 457–466, 2010.

[18] P. A. Cawood, C. J. Hawkesworth, S. A. Pisarevsky, B. Dhuime, F. A. Capitanio, and O. Nebel, "Geological archive of the onset of plate tectonics," *Philosophical Transactions of the Royal Society A: Mathematical, Physical and Engineering Sciences*, vol. 376, no. 2132, article 20170405, 2018.

[19] C. J. Hawkesworth, P. A. Cawood, and B. Dhuime, "The evolution of the continental crust and the onset of plate tectonics," *Frontiers in Earth Science*, vol. 8, p. 326, 2020.

[20] J. Korenaga, "Estimating the formation age distribution of continental crust by unmixing zircon ages," *Earth and Planetary Science Letters*, vol. 482, pp. 388–395, 2018.

[21] D. J. DePaolo, "Age dependence of the composition of continental crust: evidence from Nd isotopic variations in granitic rocks," *Earth and Planetary Science Letters*, vol. 90, no. 3, pp. 263–271, 1988.

[22] W. L. Griffin, N. J. Pearson, E. Belousova et al., "The Hf isotope composition of cratonic mantle: LAM-MC-ICPMS analysis of zircon megacrysts in kimberlites," *Geochimica et Cosmochimica Acta*, vol. 64, no. 1, pp. 133–147, 2000.

[23] E. Hasenstab, J. Tusch, C. Schnabel et al., "Evolution of the early to late Archean mantle from Hf-Nd-Ce isotope systematics in basalts and komatiites from the Pilbara Craton," *Earth and Planetary Science Letters*, vol. 553, p. 116627, 2021.

[24] J. D. Vervoort and A. I. S. Kemp, "Clarifying the zircon Hf isotope record of crust–mantle evolution," *Chemical Geology*, vol. 425, pp. 65–75, 2016.

[25] C. M. Fisher and J. D. Vervoort, "Using the magmatic record to constrain the growth of continental crust—the Eoarchean zircon Hf record of Greenland," *Earth and Planetary Science Letters*, vol. 488, pp. 79–91, 2018.

[26] A. Petersson, A. I. S. Kemp, C. M. Gray, and M. J. Whitehouse, "Formation of early Archean Granite-Greenstone Terranes from a globally chondritic mantle: insights from igneous rocks of the Pilbara Craton, Western Australia," *Chemical Geology*, vol. 551, p. 119757, 2020.

[27] R. Salerno, J. Vervoort, C. Fisher, A. Kemp, and N. Roberts, "The coupled Hf-Nd isotope record of the early Earth in the Pilbara Craton," *Earth and Planetary Science Letters*, vol. 572, p. 117139, 2021.

[28] D. R. Nelson, A. F. Trendall, and W. Altermann, "Chronological correlations between the Pilbara and Kaapvaal cratons," *Precambrian Research*, vol. 97, no. 3–4, pp. 165–189, 1999.

[29] A. H. Hickman, "Review of the Pilbara Craton and Fortescue Basin, Western Australia: crustal evolution providing environments for early life: Pilbara Craton and Fortescue Basin," *Island Arc*, vol. 21, no. 1, pp. 1–31, 2012.

[30] M. J. Van Kranendonk, R. H. Smithies, A. H. Hickman, and D. C. Champion, "Chapter 4.1 Paleoarchean Development of a Continental Nucleus: the East Pilbara Terrane of the Pilbara Craton, Western Australia," in *Developments in Precambrian Geology*, vol. 15, pp. 307–337, Elsevier, 2007.

[31] M. Van Kranendonk, *Revised Lithostratigraphy of Archean Supracrustal and Intrusive Rocks in the Northern Pilbara Craton, Western Australia*, Geological Survepy of Western Australia, 2006.

[32] A. Petersson, A. I. S. Kemp, A. H. Hickman, M. J. Whitehouse, L. Martin, and C. M. Gray, "A new 3.59 Ga magmatic suite and a chondritic source to the east Pilbara Craton," *Chemical Geology*, vol. 511, pp. 51–70, 2019.

[33] N. J. Gardiner, A. H. Hickman, Y. Lu, M. T. D. Wingate, C. L. Kirkland, and T. E. Johnson, *New Hf Isotope Insights into the Paleaoarchean Magmatic Evolution of the Mount Edgar Dome, Pilbara Craton: Implications for Early Earth and Crust Formation Processes*, Geological Survey of Western Australia, 2018.

[34] N. J. Gardiner, A. H. Hickman, C. L. Kirkland, Y. Lu, T. Johnson, and J.-X. Zhao, "Processes of crust formation in the early Earth imaged through Hf isotopes from the East Pilbara Terrane," *Precambrian Research*, vol. 297, pp. 56–76, 2017.

[35] D. Wiemer, C. E. Schrank, D. T. Murphy, L. Wenham, and C. M. Allen, "Earth's oldest stable crust in the Pilbara Craton formed by cyclic gravitational overturns," *Nature Geoscience*, vol. 11, no. 5, pp. 357–361, 2018.

[36] M. J. Van Kranendonk, R. Hugh Smithies, A. H. Hickman, and D. C. Champion, "Review: secular tectonic evolution of Archean continental crust: interplay between horizontal and vertical processes in the formation of the Pilbara Craton, Australia," *Terra Nova*, vol. 19, no. 1, pp. 1–38, 2007.

[37] A. Hickman, *Archaean Diapirism in the Pilbara Block*, 1984.

[38] R. H. Smithies, D. C. Champion, and M. J. Van Kranendonk, "Chapter 4.2 The Oldest Well-Preserved Felsic Volcanic Rocks on Earth: Geochemical Clues to the Early Evolution of the Pilbara Supergroup and Implications for the Growth of a Paleoarchean Protocontinent," in *Developments in Precambrian Geology*, vol. 15, pp. 339–367, Elsevier, 2007.

[39] D. R. Nelson, A. F. Trendall, and W. Altermann, "Erratum to 'Chronological correlations between the Pilbara and Kaapvaal cratons," *Precambrian Research*, vol. 112, no. 3–4, pp. 331-332, 2001.

[40] A. H. Hickman, "Two contrasting granite–greenstone terranes in the Pilbara Craton, Australia: evidence for vertical and horizontal tectonic regimes prior to 2900Ma," *Precambrian Research*, vol. 131, no. 3-4, pp. 153–172, 2004.

[41] A. H. Hickman and M. J. Van Kranendonk, "Early Earth evolution: evidence from the 3.5-1.8 Ga geological history of the Pilbara region of Western Australia," *Episodes*, vol. 35, no. 1, pp. 283–297, 2012.

[42] J. H. Bédard, L. B. Harris, and P. C. Thurston, "The hunting of the snArc," *Precambrian Research*, vol. 229, pp. 20–48, 2013.

[43] W. J. Collins, "Polydiapirism of the Archean Mount Edgar Batholith, Pilbara Block, Western Australia," *Precambrian Research*, vol. 43, no. 1–2, pp. 41–62, 1989.

[44] M. Van Kranendonk and W. Collins, "A review of the evidence for vertical tectonics in the Archean Pilbara Craton, Western Australia [ext. abs.]," *Australian Geoscience Survey Organisation — Geoscience Australia Records*, vol. 37, pp. 365–367, 2001.

[45] M. J. Van Kranendonk, R. H. Smithies, W. L. Griffin et al., "Making it thick: a volcanic plateau origin of Palaeoarchean continental lithosphere of the Pilbara and Kaapvaal cratons," *Geological Society of London, Special Publication*, vol. 389, no. 1, pp. 83–111, 2015.

[46] D. C. Champion and R. H. Smithies, "Chapter 4.3 Geochemistry of Paleoarchean Granites of the East Pilbara Terrane, Pilbara Craton, Western Australia: Implications for Early Archean Crustal Growth," in *Developments in Precambrian Geology*, vol. 15, pp. 369–409, Elsevier, 2007.

[47] M. J. Pawley, M. J. Van Kranendonk, and W. J. Collins, "Interplay between deformation and magmatism during doming of the Archaean Shaw granitoid complex, Pilbara Craton, Western Australia," *Precambrian Research*, vol. 131, no. 3–4, pp. 213–230, 2004.

[48] M. E. Barley and A. L. Pickard, "An extensive, crustally-derived, 3325 to 3310 Ma silicic volcanoplutonic suite in the eastern Pilbara Craton: evidence from the Kelly Belt, McPhee Dome and Corunna Downs Batholith," *Precambrian Research*, vol. 96, no. 1–2, pp. 41–62, 1999.

[49] D. C. Champion and D. L. Huston, "Radiogenic isotopes, ore deposits and metallogenic terranes: novel approaches based on regional isotopic maps and the mineral systems concept," *Ore Geology Reviews*, vol. 76, pp. 229–256, 2016.

[50] R. Smithies, D. Champion, and K. Cassidy, "Formation of Earth's early Archaean continental crust," *Precambrian Research*, vol. 127, no. 1–3, pp. 89–101, 2003.

[51] J. Carignan, P. Hild, G. Mevelle, J. Morel, and D. Yeghicheyan, "Routine analyses of trace elements in geological samples using flow injection and low pressure on-line liquid chromatography coupled to ICP-MS: a study of geochemical reference materials BR, DR-N, UB-N, AN-G and GH," *Geostandards and Geoanalytical Research*, vol. 25, no. 2–3, pp. 187–198, 2001.

[52] C. Paton, J. D. Woodhead, J. C. Hellstrom, J. M. Hergt, A. Greig, and R. Maas, "Improved laser ablation U-Pb zircon geochronology through robust downhole fractionation correction," *Geochemistry, Geophysics, Geosystems*, vol. 11, no. 3, 2010.

[53] C. Paton, J. Hellstrom, B. Paul, J. Woodhead, and J. Hergt, "Iolite: freeware for the visualisation and processing of mass

spectrometric data," *Journal of Analytical Atomic Spectrometry*, vol. 26, no. 12, p. 2508, 2011.

[54] J. A. Petrus and B. S. Kamber, "VizualAge: a novel approach to laser ablation ICP-MS U-Pb geochronology data reduction," *Geostandards and Geoanalytical Research*, vol. 36, no. 3, pp. 247–270, 2012.

[55] M. Wiedenbeck, P. Allé, F. Corfu et al., "Three natural zircon standards for u-TH-PB, LU-HF, trace element and REE analyses," *Geostandards and Geoanalytical Research*, vol. 19, no. 1, pp. 1–23, 1995.

[56] P. Vermeesch, "IsoplotR: a free and open toolbox for geochronology," *Geoscience Frontiers*, vol. 9, no. 5, pp. 1479–1493, 2018.

[57] M. M. Santos, C. Lana, R. Scholz et al., "A new appraisal of Sri Lankan BB zircon as a reference material for LA-ICP-MS U-Pb geochronology and Lu-Hf isotope tracing," *Geostandards and Geoanalytical Research*, vol. 41, no. 3, pp. 335–358, 2017.

[58] J. Sláma, J. Košler, D. J. Condon et al., "Plešovice zircon — a new natural reference material for U–Pb and Hf isotopic microanalysis," *Chemical Geology*, vol. 249, no. 1–2, pp. 1–35, 2008.

[59] A. R. Tegtmeyer and A. Kröner, "U-pb zircon ages bearing on the nature of early Archaean greenstone belt evolution, Barberton Mountainland, Southern Africa," *Precambrian Research*, vol. 36, no. 1, pp. 1–20, 1987.

[60] C. M. Fisher, J. M. Hanchar, S. D. Samson et al., "Synthetic zircon doped with hafnium and rare earth elements: a reference material for in situ hafnium isotope analysis," *Chemical Geology*, vol. 286, no. 1–2, pp. 32–47, 2011.

[61] N.-C. Chu, R. N. Taylor, V. Chavagnac et al., "Hf isotope ratio analysis using multi-collector inductively coupled plasma mass spectrometry: an evaluation of isobaric interference corrections," *Journal of Analytical Atomic Spectrometry*, vol. 17, no. 12, pp. 1567–1574, 2002.

[62] J. D. Vervoort, P. J. Patchett, U. Söderlund, and M. Baker, "Isotopic composition of Yb and the determination of Lu concentrations and Lu/Hf ratios by isotope dilution using MC-ICPMS: isotopic composition of YB," *Geochemistry, Geophysics, Geosystems*, vol. 5, no. 11, 2004.

[63] P. J. Patchett and M. Tatsumoto, "A routine high-precision method for Lu-Hf isotope geochemistry and chronology," *Contributions to Mineralogy and Petrology*, vol. 75, no. 3, pp. 263–267, 1981.

[64] J. D. Woodhead and J. M. Hergt, "A preliminary appraisal of seven natural zircon reference materials for in situ Hf isotope determination," *Geostandards and Geoanalytical Research*, vol. 29, no. 2, pp. 183–195, 2005.

[65] L. P. Black, S. L. Kamo, C. M. Allen et al., "TEMORA 1: a new zircon standard for Phanerozoic U–Pb geochronology," *Chemical Geology*, vol. 200, no. 1–2, pp. 155–170, 2003.

[66] U. Söderlund, P. J. Patchett, J. D. Vervoort, and C. E. Isachsen, "The 176Lu decay constant determined by Lu–Hf and U–Pb isotope systematics of Precambrian mafic intrusions," *Earth and Planetary Science Letters*, vol. 219, no. 3-4, pp. 311–324, 2004.

[67] A. Bouvier, J. D. Vervoort, and P. J. Patchett, "The Lu–Hf and Sm–Nd isotopic composition of CHUR: constraints from unequilibrated chondrites and implications for the bulk composition of terrestrial planets," *Earth and Planetary Science Letters*, vol. 273, no. 1–2, pp. 48–57, 2008.

[68] I. R. Williams and L. Bagas, *Geology of the Mount Edgar 1: 100 000 Sheet*, Geological Survey of Western Australia, 2007.

[69] O. Laurent, H. Martin, J. F. Moyen, and R. Doucelance, "The diversity and evolution of late-Archean granitoids: evidence for the onset of 'modern-style' plate tectonics between 3.0 and 2.5Ga," *Lithos*, vol. 205, pp. 208–235, 2014.

[70] Z. Guo and M. Wilson, "The Himalayan leucogranites: constraints on the nature of their crustal source region and geodynamic setting," *Gondwana Research*, vol. 22, no. 2, pp. 360–376, 2012.

[71] J. Halla, J. van Hunen, E. Heilimo, and P. Hölttä, "Geochemical and numerical constraints on Neoarchean plate tectonics," *Precambrian Research*, vol. 174, no. 1–2, pp. 155–162, 2009.

[72] F. Barker, "Trondhjemite: definition, environment and hypotheses of origin," in *Developments in Petrology*, vol. 6, pp. 1–12, Elsevier, 1979.

[73] C. Hawkesworth and T. Kemp, "A Pilbara perspective on the generation of Archaean continental crust," *Chemical Geology*, vol. 578, p. 120326, 2021.

[74] O. Laurent, J. Björnsen, J. F. Wotzlaw et al., "Earth's earliest granitoids are crystal-rich magma reservoirs tapped by silicic eruptions," *Nature Geoscience*, vol. 13, no. 2, pp. 163–169, 2020.

[75] R. S. J. Sparks, C. Annen, J. D. Blundy, K. V. Cashman, A. C. Rust, and M. D. Jackson, "Formation and dynamics of magma reservoirs," *Philosophical Transactions of the Royal Society A: Mathematical, Physical and Engineering Sciences*, vol. 377, no. 2139, article 20180019, 2019.

[76] C. Herzberg, K. Condie, and J. Korenaga, "Thermal history of the Earth and its petrological expression," *Earth and Planetary Science Letters*, vol. 292, no. 1–2, pp. 79–88, 2010.

[77] O. Nebel, F. A. Capitanio, J.-F. Moyen et al., "When crust comes of age: on the chemical evolution of Archaean, felsic continental crust by crustal drip tectonics," *Philosophical Transactions of the Royal Society A: Mathematical, Physical and Engineering Sciences*, vol. 376, no. 2132, article 20180103, 2018.

[78] A. I. S. Kemp, J. D. Vervoort, K. E. Bjorkman, and L. M. Iaccheri, "Hafnium isotope characteristics of Palaeoarchaean zircon OG 1/OGC from the Owens Gully Diorite, Pilbara Craton, Western Australia," *Geostandards and Geoanalytical Research*, vol. 41, no. 4, pp. 659–673, 2017.

[79] R. K. Workman and S. R. Hart, "Major and trace element composition of the depleted MORB mantle (DMM)," *Earth and Planetary Science Letters*, vol. 231, no. 1–2, pp. 53–72, 2005.

[80] F. Farina, C. Albert, and C. Lana, "The Neoarchean transition between medium- and high-K granitoids: clues from the Southern São Francisco Craton (Brazil)," *Precambrian Research*, vol. 266, pp. 375–394, 2015.

[81] N. J. Gardiner, J. A. Mulder, C. L. Kirkland, T. E. Johnson, and O. Nebel, "Palaeoarchaean TTGs of the Pilbara and Kaapvaal cratons compared; an early Vaalbara supercraton evaluated," *South African Journal of Geology*, vol. 124, no. 1, pp. 37–52, 2021.

[82] R. H. Smithies, D. C. Champion, and M. J. Van Kranendonk, "Formation of Paleoarchean continental crust through infracrustal melting of enriched basalt," *Earth and Planetary Science Letters*, vol. 281, no. 3-4, pp. 298–306, 2009.

[83] A. I. S. Kemp, A. H. Hickman, C. L. Kirkland, and J. D. Vervoort, "Hf isotopes in detrital and inherited zircons of

the Pilbara Craton provide no evidence for Hadean continents," *Precambrian Research*, vol. 261, pp. 112–126, 2015.

[84] V. Debaille, C. O'Neill, A. D. Brandon et al., "Stagnant-lid tectonics in early earth revealed by ^{142}Nd variations in late Archean rocks," *Earth and Planetary Science Letters*, vol. 373, pp. 83–92, 2013.

[85] A. B. Bauer, J. R. Reimink, T. Chacko, B. J. Foley, S. B. Shirey, and D. G. Pearson, "Hafnium isotopes in zircons document the gradual onset of mobile-lid tectonics," *Geochemical Perspectives Letters*, vol. 14, pp. 1–6, 2020.

[86] J. A. Mulder, O. Nebel, N. J. Gardiner, P. A. Cawood, A. N. Wainwright, and T. J. Ivanic, "Crustal rejuvenation stabilised Earth's first cratons," *Nature Communications*, vol. 12, no. 1, article 3535, 2021.

[87] A. I. S. Kemp, "Early earth geodynamics: cross examining the geological testimony," *Philosophical Transactions of the Royal Society A: Mathematical, Physical and Engineering Sciences*, vol. 376, no. 2132, article 20180169, 2018.

[88] A. H. Hickman, R. Smithies, and I. Tyler, *Evolution of Active Plate Margins: West Pilbara Superterrane, De Grey Superbasin, and the Fortescue and Hamersley Basins-a Field Guide*, Geological Survey of Western Australia, 2010.